Linear and Two-Photon Absorption in Zero- and One-Dimensional CdS Nanocrystals: Influence of Size and Shape

ARTICLE *in* THE JOURNAL OF PHYSICAL CHEMISTRY C · NOVEMBER 2013

Impact Factor: 4.77 · DOI: 10.1021/jp407453e

THE JOURNAL OF PHYSICAL CHEMISTRY C

Article

pubs.acs.org/JPCC

Linear and Two-Photon Absorption in Zero- and One-Dimensional CdS Nanocrystals: Influence of Size and Shape

Alexander W. Achtstein,*[,†] Jonas Hennig,[†] Anatol Prudnikau,[‡] Mikhail V. Artemyev,[‡] and Ulrike Woggon[†]

[†]Institut für Optik und Atomare Physik, Technische Universität Berlin, Hardenbergstrasse 36, 10623 Berlin, Germany

[‡]Institute for Physico-Chemical Problems, Belarussian State University, Leningradskaya Street 14, 220030 Minsk, Belarus

Supporting Information

ABSTRACT: Colloidal CdS nanocrystals show strongly enhanced two-photon absorption (TPA) cross sections $\delta^{(2)}$ of 10^4 to 10^5 GM over a wide NIR spectral range, making them ideal markers for confocal two-photon microscopy. We present a systematic study of the size and shape dependence of the linear and TPA cross sections for colloidal CdS dots and rods of diameters d between 2 and 5 nm. On the basis of z-scan measurements, we observe that the TPA cross section of colloidal CdS dots at 800 nm in and near the absorption continuum is manly shape and volume dependent, whereas it is less influenced by the electronic confinement. In the case of resonance to the lowest excitonic transition, a significant confinement-induced TPA enhancement with respect to the off-resonant case is observed. Colloidal CdS rods can exhibit a factor on the order of 10 larger $\delta^{(2)}$ compared to CdS dots of the same diameter. In very small CdS rods a non-negligible three-photon absorption is found and assigned to a change in valence band symmetry.

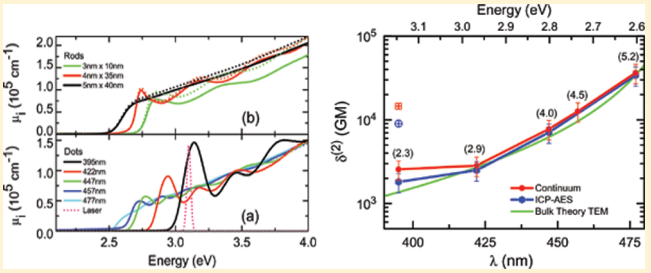

INTRODUCTION

Two-photon absorption (TPA) as an excitation method of dye markers in high-resolution microscopy has become more and more important in fields such as cell biology or medical research. As compared to standard organic dyes,[1] semiconductor nanocrystals (NCs) can reach TPA cross sections $\delta^{(2)}$ as high as $\sim 10^5$ GM with the advantage of a more compact size[2,3] and higher photostability. Therefore, semiconductor NCs are ideally suited for high-contrast two-photon microscopy, having higher depth resolution and higher TPA efficiency per volume. Wide-gap II−VI compound NCs, and here CdS in particular, are of interest since their two-photon transition energies are in the near-infrared range, allowing for large tissue penetration depths for imaging. However, a systematic study of the size or shape dependency of $\delta^{(2)}$ is still missing. Here we present a study of on- and off-resonant TPA enhancement in CdS nanodots and rods.

EXPERIMENTAL SECTION

For our experiments we use colloidal CdS NCs (dots and rods) synthesized by standard techniques[4−6] and characterized by high-resolution TEM (HR-TEM) (see the Supporting Information). To study the influence of confinement and shape on the TPA of CdS NCs, we determine in the first step the absolute NC concentrations in colloidal solution from their continuum absorption (CA) and from inductively coupled plasma atomic emission spectroscopy (ICP-AES) and derive the linear absorption cross sections $\delta^{(1)}$ of the CdS dots and rods, since there is only very little information on absorption coefficients in hexagonal CdS nanorystals[5] available. We report in the following paragraph z-scan measurements on these CdS dots and rods and analyze the transmittance $T(z)$ using fit routines for TPA and three-photon absorption (3PA) processes. Finally, the derived coefficients $\delta^{(2)}$ and $\delta^{(3)}$ are compared for dots and rods, and their size and shape dependencies are discussed and summarized.

A Lorentz local field theory in connection with an effective medium Maxwell−Garnett approach[7−9] can be applied to derive the linear absorption cross section $\delta^{(1)}$ in the continuum absorption region of the nanocrystal absorption spectrum. We model our dots as absorbing dielectric spheres and obtain

$$\delta^{(1)}_{QD} = \frac{2\omega}{n_m c} V_{QD} |f(\omega)_{QD}|^2 n_s k_s \quad (1)$$

$$f(\omega)_{QD} = 3\varepsilon_m/(2\varepsilon_m + \varepsilon_s) \quad (2)$$

with the local Lorentz field factor $f(\omega)_{QD}$. Here ε_m, n_m, and k_m denote the matrix dielectric function, refractive index, and absorption coefficient, whereas ε_s, n_s, and k_s denote the same for the CdS semiconductor. The theoretically derived absolute absorption cross section in the CA region high above the discrete states can then be used to derive the NC concentration via optical methods experimentally. Figure 1 shows the absorption spectra of our CdS dot and rod samples in chloroform solution. On the y-axis the volume-independent value of the intrinsic absorption μ_i is plotted, given by $\mu_i(E) =$

Received: July 26, 2013
Revised: October 31, 2013

   dx.doi.org/10.1021/jp407453e | J. Phys. Chem. C XXXX, XXX, XXX−XXX

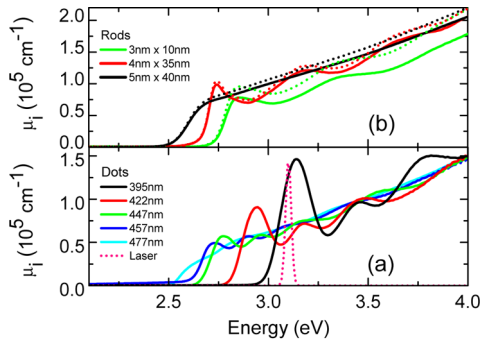

Figure 1. Intrinsic absorption spectra of the CdS dot (a) and rod (b) samples in chloroform solution. The dotted lines in (b) represent the model of the infinitely long cylinders, whereas the continuous lines represent the ellipsoid model. The dotted curve in (a) shows the 800 nm, 130 fs laser excitation used for the *z*-scan measurements, here plotted at the two-photon energy. The color-coded wavelengths in (a) denote the position of the energetically lowest absorption maximum of each spectrum of the CdS dot samples.

$\delta^{(1)}(E)/V_{QD/QR}$, with $V_{QD/QR}$ being the NC volume and $\delta^{(1)}$ the linear absorption cross section (see the Supporting Information). For the dots in our size range, we calculate according to Van Dijk et al.[10] that the scattering contribution is at least 4 orders of magnitude lower than the absorption contribution to the total intrinsic extinction coefficient. Therefore, we can neglect the scattering contribution to the total intrinsic extinction coefficient μ.

For our rods with an aspect ratio between 3.3 and 8.7, different local field factors for orientation parallel and perpendicular to the nanorod *c*-axis are obtained. We approximate the nanorods as prolate ellipsoids, for which Osborn[11] has calculated the depolarization factors L_z along and $L_{x,y}$ perpendicular to the long semiaxis[12,13] and obtain for $\delta^{(1)}_{QR}$

$$\delta^{(1)}_{QR} = \frac{2\omega}{3n_m c} V_{QR}(|f_z(\omega)|^2 n_{s\|} k_{s\|} + 2|f_{x/y}(\omega)|^2 n_{s\perp} k_{s\perp})$$

$$\text{with} \quad f_i(\omega) = \frac{1}{1 + L_i(\varepsilon_s/\varepsilon_m - 1)} \tag{3}$$

$$L_z = \frac{1}{1-p^2}\left[1 - p\frac{\arcsin(\sqrt{1-p^2})}{\sqrt{1-p^2}}\right]$$

$$L_{x/y} = \frac{1 - L_z}{2} \tag{4}$$

with the semiconductor refractive index $n_{s\|/\perp}$ and extinction $k_{s\|/\perp}$ (along and perpendicular to the *c*-axis) and their directional averages $n_s = (n_{s\|} + 2n_{s\perp})/3$ and k_s.

We determine the concentration of our nanoparticles also by ICP-AES measurements and compare them with the concentrations calculated via their intrinsic CA coefficients at 4.0 eV by eqs 3 and 4 using bulk dielectric function data for CdS[14] and our solvent chloroform[15] (see also the Supporting Information). In this case we estimate the concentration error to be 26% for ICP-AES and in the same range for the CA method. The good agreement in both ICP-AES and CA methods (see also the TPA measurements in Figure 3) further substantiates our CA model, and we normalize the experimental absorption spectra to the CA method values at 4.0 eV, resulting in Figure 1. Figure 1b also shows the results when modeling the CdS rods as infinitely long cylinders. We find an aspect ratio dependence for the intrinsic absorption μ_i in the ellipsoid model (continuous lines) as compared to the infinite cylinder model (dotted lines) (see also the Supporting Information). In the following sections we use the ellipsoidal model.

To study two-photon absorption in our CdS NCs, we apply *z*-scan measurements with a regeneratively amplified τ_{fwhm} = 130 fs Ti:Sa laser system with a 1 kHz repetition rate at 800 nm. An f_L = 20 cm lens has been used to create a 43 μm diameter Gaussian beam waist (characterized by beam profiling) through which a 1 or 2 mm optical path length fused silica cuevette is moved by a motorized translation stage. The absorption changes are measured as the ratio of the transmitted beam to a reference beam intensity. The obtained open *z*-scan relative transmission curves $T(z)$ were further analyzed using numerical fit functions for two- and three-photon absorption on the basis of refs 16 and 17 (see the Supporting Information).

RESULTS AND DISCUSSION

The results of the open-aperture *z*-scans for CdS core nanoparticles capped with TOPO (trioctylphosphine oxide) are displayed in Figure 2 along with the best fitting curves for

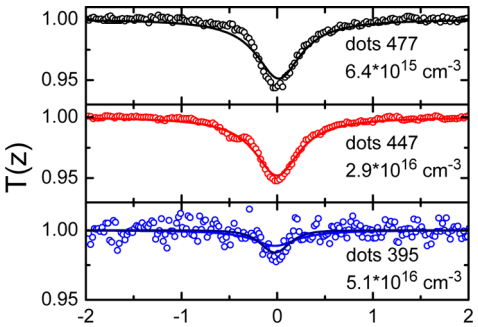

Figure 2. *z*-scan transmission with a pulse peak power density of 158 GW/cm^2 for three different dot sizes (the first exciton absorption wavelength is given in the plot labels). The nanoparticle concentrations in chloroform solutions are derived from the CA method as described in the text. The solid lines in data point color reflect the TPA fits, whereas the navy-colored line for the 395 nm dots corresponds to a 3PA fit.

TPA and 3PA. The obtained data of the TPA cross sections $\delta^{(2)}$ are plotted in Figure 3 versus the wavelength of the first exciton absorption peak for a set of five different sizes of spherical CdS NCs. For the dots absorbing at 395 and 457 nm, we observe a significant three-photon absorption contribution. The resulting 3PA cross sections are $\delta^{(3)} = 5.0 \times 10^{-76}$ (cm^6 s^2)/photon (457 nm dots) and 1.8×10^{-76} (cm^6 s^2)/photon (395 nm dots) when fitted with a 3PA model. (For details on how $\delta^{(2)}$ and $\delta^{(3)}$ are derived from $T(z)$ scans using the NC concentrations determined by the CA and ICP-AES methods, see also the Supporting Information.) We observe excellent agreement of the CA method results (red curve) with the ICP-AES results (blue curve) for the intermediate and large size ranges (which further justifies the use of bulk diectric constants at 4 eV in our calculations). There is also good agreement in the intermediate size range of our TPA results with those of Li at al.[2] (measuring in the nanocrystal absorption range of 430−451 nm). The deviations of the ICP-AES and CA models for the 395 nm sample may be attributed to the fact that there is still a contribution of quantized state absorption at 4.0 eV in the 395

dx.doi.org/10.1021/jp407453e | J. Phys. Chem. C XXXX, XXX, XXX−XXX

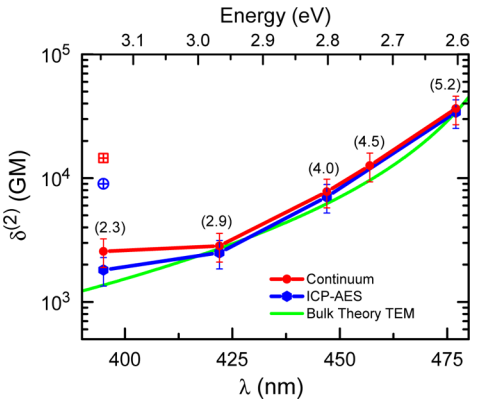

Figure 3. Two-photon absorption cross sections of CdS nanocrystals derived from Figure 2 versus the first exciton absorption wavelength along with the corresponding nanocrystal diameters (nm). Evaluation of particle concentrations is done by CA including TEM-derived sizes (red curve) and ICP-AES (blue curve). Using the bulk TPA coefficient at 800 nm for energies in the continuum absorption, the green curve represents the volume scaling of $\delta^{(2)}$ with respect to eq 5 for the TEM-derived sizing curve. The crossed symbols correspond to the effectively optically active part of the 395 nm dot population (for an explanation see the text).

nm sample, leading to an underestimation of intrinsic absorption (a normalization at higher energies will not increase the accuracy because of the onset of ligand and solvent absorption for energies significantly above 4 eV).

To discuss the dependence of $\delta^{(2)}$ on the NC diameter and the corresponding first excitonic absorption energy (wavelength), our TEM data are fitted by $E_g = hc/\lambda = E_{g,bulk} + b/d^p$ with empirical constants $b = 2.448$ and $p = 1.607$, d given in nanometers, and $E^A_{g,bulk} = 2.482$ eV (fixed, from ref 14). Furthermore, we add in Figure 3 the scaling law for the bulk TPA coefficient $\delta^{(2)}$ at 800 nm (green curve) using eq 5 proposed by Blanton et al.:[18]

$$\delta^{(2)} = h\omega\beta_{bulk}\left(\frac{3\varepsilon_m}{2\varepsilon_m + \varepsilon_s}\right)^4 \frac{N}{n_c} \quad (5)$$

Here ω corresponds to the exciting laser angular frequency at 800 nm, N the number of unit cells per particle, n_c the volume density of unit cells in the bulk, and $\beta_{bulk} = 8.8$ cm/GW[19] the bulk TPA coefficient.

Two significant results can be derived from Figure 3: (i) The TPA cross section $\delta^{(2)}$ of CdS dots shows a volume scaling law similar to that of bulk CdS. Since $N \sim d^3$ is valid for eq 5, the cross sections tend to increase with the third power of the NC radius, leading to an increase of the TPA cross section with increasing first exciton absorption wavelength. (ii) The experimental values of $\delta^{(2)}$ for CdS dots are in good agreement with the expected two-photon absorption cross sections calculated by eq 5 so that we observe a dominant volume scaling. This is in good qualitative agreement with the volume scaling behavior of the TPA cross sections of dot in rod CdSe/CdS particles recently reported by Allione et al.[20]

The two crossed symbols in Figure 3 correspond to the effectively optically active part of the 395 nm dot population with respect to the 800 nm, 130 fs laser excitation. Since the inhomogeneous broadening (homogeneous line width of single emitter <10 meV) of the first exciton energies is larger than the 12 nm fwhm of the Ti:Sa laser (Figure 1), the laser pulses interact only with a part of the nanoparticle ensemble. In the resonant case of our 395 nm dots, it is possible to relate the measured cross section to the optically interacting subensemble of the dots. Therefore, we calculate the overlap integral of the squared laser profile with the squared first excitonic absorption, fitting the data in Figure 1 by Voigt profiles. This results in only 18% of all 395 nm nanocrystals interacting with the 800 nm laser pulses. Considering only the interacting subensemble, the TPA cross section is increased by a factor of 5.6 (indicated with crossed symbols in Figure 3). Due to the spectral overlap of inhomogeneously broadened higher states, this renormalization cannot be done with excited states.

The importance of inhomogeneous broadening has not yet been taken into account in the present papers on CdS nanoparticles,[2,16,19] which report a broad range of TPA cross sections. Additionally, the usage of near-Fourier-limited pulses leads to a significant alteration of the pulse line width if measurements are performed with different temporal pulse widths. As a result, the obtained TPA coefficients are different when the pulse width changes, even for the same peak powers. Since different femtosecond laser systems have different time–bandwidth products ($\Delta T\Delta\nu = [2\ln(2)]/\pi \approx 0.44$ for Gaussian and $\Delta T\Delta\nu = (4\ \mathrm{arccosh}^2\ \sqrt{2})/\pi^2 \approx 0.31$ for sech^2 envelope functions), different TPA cross sections can be obtained even using the same temporal pulse width ΔT and peak intensity. This might be the reason, besides different size distributions, why measured cross sections in the literature strongly deviate from each other; e.g., for 4 nm diameter CdS particles published data are 7000 GM/250 fs,[21] 7900 GM/140 fs,[19] 3500 GM/100 fs (extrapolated),[2] and 10 000 GM/90 fs[22] at 800 nm.

In the next section we investigate CdS rods with diameters similar to those of our dots to compare the results of dots and rods. Figure 4 shows the experimental data $T(z)$ of our CdS

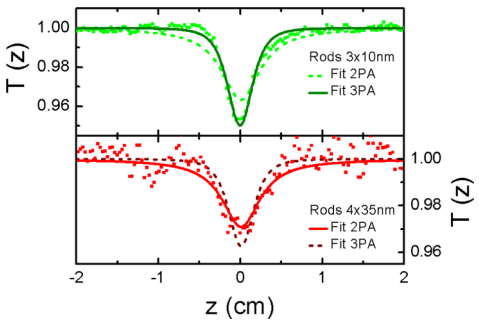

Figure 4. Open-aperture z-scan traces for different rods with 154 (3 × 10 nm) and 164 (4 × 35 nm) GW/cm^2 peak intensities at 800 nm with concentrations of 2.0×10^{15} and 1.14×10^{15} cm^{-3} measured in chloroform solution.

rods with 3 × 10 and 4 × 35 nm size and concentrations of 2.44×10^{15} and 1.21×10^{15} cm^{-3} (ellipsoidal model), respectively. The solid and dashed lines correspond to least-squares fits of TPA and 3PA absorption cross sections according to refs 16 and 17 (see the Supporting Information). Interestingly, the stronger quantized 3 × 10 nm rods exhibit predominant 3PA with a cross section of $\delta^{(3)}_{3\times10,El} = 1.8 \times 10^{-74}$ (cm^6 s^2)/photon in the ellipsoidal model, whereas the less quantized 4 × 35 nm rods show TPA at this power density with $\delta^{(2)}_{4\times35,El} = 1.9 \times 10^5$ GM. The measured TPA cross section is in good agreement with the expected TPA cross section of 4 × 35 nm CdS rods calculated with the local field factors in eqs 3 and 4 analogous to eq 5. A value of 2.06×10^5 GM for the 4 × 35 nm rods is expected from these calculations, which agrees well with our

dx.doi.org/10.1021/jp407453e | J. Phys. Chem. C XXXX, XXX, XXX–XXX

experimental finding within the 26% error of our experimental results. Some authors[2] further multiply the obtained rod TPA cross section by a factor of 5 to account for the random orientation of rods in the solution and give the maximum possible value for the nonlinearity for parallel orientation. It is still unknown why the 3 × 10 nm rods show predominant 3PA while the less confined 4 × 35 nm and most other dots show predominant TPA. This might be related to different selection rules for TPA and 3PA transitions (see also the Supporting Information). One-photon transitions, TPA, and 3PA access completely different manifolds of electronic transitions.[23] As for CdSe rods[24,25] and platelets,[26] valence band mixing plays an important role in CdS rods.

According to calculations of Planelles et al.,[27] the symmetry of the lowest valence band state is always F_z = 1/2 (p-like symmetry) for small-diameter rods (diameter 3 nm) and F_z = 3/2 (s-like symmetry) for larger diameter rods (e.g., 4 × 35 nm) with fine structure splittings on the order of 10 meV. This change in symmetry might also affect the exited states resonant to the 800 nm two-photon excitation, leading to different allowed TPA transitions for small and large rods.

It can be assumed that for the smallest 3 × 10 nm rods the TPA transition at 800 nm is not allowed, whereas a higher transition is resonant to three photons and dipole allowed. It is difficult to attribute the relevant transitions to the rod's absorption spectra, since higher states show less pronounced absorption peaks and the spectra become more and more structureless due to continuum absorption (see the Supporting Information). Further calculations of the hole band mixing in CdS dots and rods by Planelles et al.[27] have shown that for dots a ground-state crossover of the valence band states with F_z = 1/2 and F_z = 3/2 (being the energetically lowest state for large radii) exists at d = 9 nm. In contrast to that and CdSe nanorods,[28] there is no symmetry crossover with increasing aspect ratio for CdS rods.[27] Instead the ground-state symmetry is always that of the QDs: F_z = 1/2 for rods with small diameters (e.g., d = 3 nm as in the 3 × 10 nm rods) and F_z = 3/2 for rods with weak radial confinement. (For our 3 × 10 nm rods an exchange splitting of ∼30 meV is expected.[27]). The predicted change in valence band symmetry might have an impact on our two- and three-photon absorption properties via selection rules blocking TPA for the 3 × 10 nm rods and 3PA for the 4 × 35 nm rods.

CONCLUSION

In summary, we have explored the two- and three-photon absorption properties of CdS nanoparticles suitable for confocal two-photon microscopy. For the CdS dots we have seen that the size scaling and particle shape have the main influence on the observed TPA cross sections, whereas the electronic confinement leads only in the case of resonance to the lowest exciton state to a significant TPA enhancement. The observed volume scaling of the TPA coefficient at 800 nm is in good agreement with theoretical TPA cross section calculations for large dots and rods. It has been further shown that the exciting laser bandwidth plays an important role in the determination of the TPA cross sections in an inhomogeneously broadened ensemble.

ASSOCIATED CONTENT

Supporting Information

Size distributions of the CdS particles from TEM, definition of the intrinsic absorption coefficient, z-scan theory for two- and three-photon absorption, and impact of selection rules on the two- and three-photon absorption process. This material is available free of charge via the Internet at http://pubs.acs.org

AUTHOR INFORMATION

Corresponding Author

*E-mail: alexander.achtstein@tu-berlin.de.

Notes

The authors declare no competing financial interest.

ACKNOWLEDGMENTS

Financial support is acknowledged from DFG Priority Program SPP1165 Nanowires.

REFERENCES

(1) Makarov, N. S.; Campo, J.; Hales, J. M.; Perry, J. W. Rapid, Broadband Two-Photon-Excited Fluorescence Spectroscopy and Its Application to Red-Emitting Secondary Reference Compounds. *Opt. Mater. Express* **2011**, *1*, 551−563.

(2) Li, X.; van Embden, J.; Chon, J. W. M.; Gu, M. Enhanced Two-Photon Absorption of CdS Nanocrystal Rods. *Appl. Phys. Lett.* **2009**, *94*, 103117.

(3) Gao, Y.; Tonizzo, A.; Walser, A.; Potasek, M.; Dorsinville, R. Enhanced Optical Nonlinearity of Surfactant-Capped CdS Quantum Dots Embedded in an Optically Transparent Polystyrene Thin Film. *Appl. Phys. Lett.* **2008**, *92*, 033106−1−3.

(4) Yu, W. W.; Peng, X. Formation of High-Quality CdS and Other IIVI Semiconductor Nanocrystals in Noncoordinating Solvents: Tunable Reactivity of Monomers. *Angew. Chem., Int. Ed.* **2002**, *41*, 2368−2371.

(5) Yu, W. W.; Qu, L.; Guo, W.; Peng, X. Experimental Determination of the Extinction Coefficient of CdTe, CdSe, and CdS Nanocrystals. *Chem. Mater.* **2003**, *15*, 2854−2860.

(6) Ghezelbash, A.; Koo, B.; Korgel, B. A. Self-Assembled Stripe Patterns of CdS Nanorods. *Nano Lett.* **2006**, *6*, 1832−1836.

(7) Moreels, I.; Lambert, K.; Smeets, D.; De Muynck, D.; Martins, J. C.; Vanhaecke, F.; Vantomme, A.; Delerue, C.; Allan, G.; Hens, Z. Size-Dependent Optical Properties of Colloidal PbS Quantum Dots. *ACS Nano* **2009**, *3*, 3023−3030.

(8) Leatherdale, C. A.; Woo, W. K.; Mikulec, F. V.; Bawendi, M. G. On the Absorption Cross Section of CdSe Nanocrystal Quantum Dots. *J. Phys. Chem. B* **2002**, *106*, 7619−7622.

(9) Jasieniak, J.; Smith, L.; Embden, J. v.; Mulvaney, P.; Califano, M. Re-examination of the Size-Dependent Absorption Properties of CdSe Quantum Dots. *J. Phys. Chem. C* **2009**, *113*, 19468−19474.

(10) van Dijk, M. A.; Tchebotareva, A. L.; Orrit, M.; Lippitz, M.; Berciaud, S.; Lasne, D.; Cognet, L.; Lounis, B. Absorption and Scattering Microscopy of Single Metal Nanoparticles. *Phys. Chem. Chem. Phys.* **2006**, *8*, 3486−3495.

(11) Osborn, J. A. Demagnetizing Factors of a General Elliipsoid. *Phys. Rev.* **1945**, *67*, 351−357.

(12) Sihvola, A. Dielectric Polarization and Particle Shape Effects. *J. Nanomater.* **2007**, *2007*, 1−9.

(13) Perova, T. S. The Effect of Local Field Dispersion on the Spectral Characteristics of Nanosized Particles and Their Composites. In *Fourier Transforms—Approach to Scientific Principles*; Nikolic, G., Ed.; InTech: Rijeka, Croatia, 2011.

(14) Blachnik, R.; Chu, J.; Galazka, R.; Geurts, J.; Gutowski, J.; Hoenerlage, B.; Hofmann, D.; Kossut, J.; Levy, R.; Michler, P. *Landolt-Boernstein, New Series*; Springer: New York, 1999; Vol. *III/41B*.

(15) Samoc, A. Dispersion of Refractive Properties of Solvents: Chloroform, Toluene, Benzene, and Carbon Disulfide in Ultraviolet, Visible, and Near-Infrared. *J. Appl. Phys.* **2003**, *94*, 6167−6174.

(16) He, J.; Qu, Y.; Li, H.; Mi, J.; Ji, W. Three-Photon Absorption in ZnO and ZnS Crystals. *Opt. Express* **2005**, *13*, 9235−9247.

(17) Rumi, M.; Perry, J. W. Two-Photon Absorption: An Overview of Measurements and Principles. *Adv. Opt. Photonics* **2010**, *2*, 451−518.
(18) Blanton, S. A.; Dehestani, A.; Lin, P. C.; Guyot-Sionnest, P. Photoluminescence of Single Semiconductor Nanocrystallites by Two-Photon Excitation Microscopy. *Chem. Phys. Lett.* **1994**, *229*, 317−322.
(19) He, J.; Mi, J.; Li, H.; Ji, W. Observation of Interband Two-Photon Absorption Saturation in CdS Nanocrystals. *J. Phys. Chem. B* **2005**, *109*, 19184−19187.
(20) Allione, M.; Ballester, A.; Li, H.; Comin, A.; Movilla, J. L.; Climente, J. I.; Manna, L.; Moreels, I. Two-Photon-Induced Blue Shift of Core and Shell Optical Transitions in Colloidal CdSe/CdS Quasi-Type II Quantum Rods. *ACS Nano* **2013**, *7*, 2443−2452.
(21) He, J.; Ji, W.; Ma, G. H.; Tang, S. H.; Kong, E. S. W.; Chow, S. Y.; Zhang, X. H.; Hua, Z. L.; Shi, J. L. Ultrafast and Large Third-Order Nonlinear Optical Properties of CdS Nanocrystals in Polymeric Film. *J. Phys. Chem. B* **2005**, *109*, 4373−4376.
(22) Gu, B.; Wang, J.; Chen, J.; Fan, Y.-X.; Ding, J.; Wang, H.-T. Z-Scan Theory for Material with Two- and Three-Photon Absorption. *Opt. Express* **2005**, *13*, 9230−9234.
(23) Schmidt, M. E.; Blanton, S. A.; Hines, M. A.; Guyot-Sionnest, P. Size-Dependent Two-Photon Excitation Spectroscopy of CdSe Nanocrystals. *Phys. Rev. B* **1996**, *53*, 12629−12632.
(24) Le Thomas, N.; Herz, E.; Schöps, O.; Woggon, U.; Artemyev, M. V. Exciton Fine Structure in Single CdSe Nanorods. *Phys. Rev. Lett.* **2005**, *94*, 016803.
(25) Shabaev, A.; Efros, A. L. 1D Exciton Spectroscopy of Semiconductor Nanorods. *Nano Lett.* **2004**, *4*, 1821−1825.
(26) Achtstein, A. W.; Schliwa, A.; Prudnikau, A.; Hardzei, M.; Artemyev, M. V.; Thomsen, C.; Woggon, U. Electronic Structure and Exciton-Phonon Interaction in Two-Dimensional Colloidal CdSe Nanosheets. *Nano Lett.* **2012**, *12*, 3151−3157.
(27) Planelles, J.; Rajadell, F.; Climente, J. I. Hole Band Mixing in CdS and CdSe Quantum Dots and Quantum Rods. *J. Phys. Chem. C* **2010**, *114*, 8337−8342.
(28) Zhao, Q.; Graf, P. A.; Jones, W. B.; Franceschetti, A.; Li, J.; Wang; Kim, K. Shape Dependence of Band-Edge Exciton Fine Structure in CdSe Nanocrystals. *Nano Lett.* **2007**, *7*, 3274−3280.